Evidence for rapid hydrolysis of shoot-derived sucrose using an ultrasensitive ratiometric matryoshka-type MGlucoMeter sensor

Yuuma Ishikawa, Nora Zöllner, Susanne Paradies und Wolf B. Frommer

Article - Version of Record

Suggested Citation:
Ishikawa, Y., Zöllner, N., Paradies, S., & Frommer, W. B. (2026). Evidence for rapid hydrolysis of shoot-derived sucrose using an ultrasensitive ratiometric matryoshka-type MGlucoMeter sensor. The plant journal, 125(5), Article e70778. https://doi.org/10.1111/tpj.70778

the plant journal

SEB SOCIETY FOR EXPERIMENTAL BIOLOGY

The Plant Journal (2026) **125,** e70778 doi: 10.1111/tpj.70778

TECHNICAL ADVANCE

Evidence for rapid hydrolysis of shoot-derived sucrose using an ultrasensitive ratiometric matryoshka-type MGlucoMeter sensor

Yuuma Ishikawa[1,2,*,†], Nora Zöllner[1], Susanne Paradies[1] and Wolf B. Frommer[1,2,3,*]

[1]*Faculty of Mathematics and Natural Sciences, Institute for Molecular Physiology, Heinrich Heine University Düsseldorf, Düsseldorf, Germany,*

[2]*Cluster of Excellence on Plant Sciences (CEPLAS), Heinrich Heine University, Düsseldorf, Germany, and*

[3]*Institute for Transformative Biomolecules, ITbM, Nagoya University, Nagoya, Japan*

Received 27 September 2025; revised 19 December 2025; accepted 12 February 2026.

*For correspondence (e-mail y-ishikawa-503@g.ecc.u-tokyo.ac.jp and frommew@hhu.de).

[†]Present address: Department of Biological Sciences, School of Sciences, University of Tokyo, Tokyo, Japan

SUMMARY

To enable sensitive *in vivo* monitoring of the glucose transport and metabolism, we developed a series of ultrasensitive and ratiometric genetically encoded sensors (MGlucoMeter) by inserting a Matryoshka dual fluorophore cassette consisting of cpsfGFP (circularly permuted superfolder GFP) and LSSmApple (Large Stokes Shift mApple) into the glucose-binding protein ttGBP (*Thermus thermophilus* glucose-binding protein) from *Thermus thermophilus*. The initial MGlucoMeter1.0 version was subjected to an alanine scan of the hinge region producing the more sensitive MGlucoMeter2.6 with a glucose-induced $\Delta F/F_0$ change of 3.0, an affinity for glucose of 15 μM, and an approximate detection range of 1–215 μM. To generate variants suitable for *in vivo* measurements, a series of affinity mutants was generated by mutating two histidines predicted to be involved in substrate binding. MGlucoMeter2.6-353n (affinity 353 nM), MGlucoMeter2.6-15 μ (affinity 15 μM), MGlucoMeter2.6-700 μ (affinity 700 μM), MGlucoMeter2.6-1 m (affinity 1 mM), and MGlucoMeter2.6-7 m (affinity 7 mM) cover a combined detection range between ~40 nM–55 mM. When expressed from a ubiquitous promoter in the cytosol of the Arabidopsis gene-silencing mutant *rdr6* (RNA-dependent RNA polymerase 6), MGlucoMeter2.6-1 m reports time- and concentration-dependent accumulation of glucose in seedling roots after external addition of glucose. The sensor also detected rapid release of sugars in the root tip and rapid hydrolysis of the shoot-derived sucrose.

Keywords: technical advance.

INTRODUCTION

While metabolomics provides quantitative information on the steady-state levels of metabolites, it lacks spatial and time resolution. An alternative is the visualization of metabolite dynamics with subcellular resolution using genetically encoded sensors. The first glucose sensors (e.g., FLIPglu-600 μΔ13) were developed by sandwiching a sugar binding proteins from the family of bacterial periplasmic binding proteins between two variants of the green fluorescent proteins that had features allowing for FRET (Förster Resonance Energy Transfer) (Deuschle et al., 2005; Fehr et al., 2002; Fehr et al., 2003; Lager et al., 2006). These sensors were successfully used for monitoring glucose dynamics in bacterial and yeast cells, mammalian cells and in the plant Arabidopsis (Bermejo, Haerizadeh, et al., 2011; Chaudhuri et al., 2008; Chaudhuri et al., 2011; Deuschle et al., 2006; Kaper et al., 2008). The glucose sensors were also successfully deployed for genetic screens to identify networks involved in the regulation of glucose transport and for studying the transfer of glucose across endoplasmic reticulum membranes in mammalian HepG2 cells (Bermejo et al., 2010; Bermejo et al., 2013; Bermejo, Ewald, et al., 2011; Fehr et al., 2005; Takanaga et al., 2008). While the FRET-based approach yielded sensors suitable for *in vivo* measurements, the sensitivity of the sensors was limited due to the intrinsic coupling of the relative change in the emission of the two

fluorophores. Roger Tsien had developed an alternative approach using a circularly permutated GFP (cpGFP) as an intensiometric reporter element (Baird et al., 1999). Although the sensitivity of the intensiometric cpGFP-based sensors was higher, the FRET sensors had one major advantage: they were ratiometric and thus not impacted by changes in the sensor levels. To overcome the limitation, calcium and ammonium transporter activity sensors were generated that contained a nested large Stokes shift fluorophore (LSSmOrange) as a reference, enabling ratiometric measurements (Ast et al., 2015; Ast et al., 2017). The calcium sensor was further improved by replacing LSSmOrange with the better suited LSSmApple (Ejike et al., 2024). Since proteins from thermophilic organisms are more robust, the glucose-binding protein from *T. thermophilus* had previously been used to generate an intensiometric glucose sensors by inserting cpGFP into ttGPB (*Thermus thermophilus* glucose-binding protein) to produce iGlucoSnFR (intensity-based Glucose-Sensing Fluorescent Reporter) (Keller et al., 2021).

Here, a series of ultrasensitive glucose sensors (MGlucoMeter) was generated using the Matryoshka technology. For this purpose, the previously developed Matryoshka cassette, consisting of the superfolder variant cpsfGFP as a sensory domain and LSSmApple as a reference fluorophore (Ejike et al., 2024; Pedelacq et al., 2006), was inserted into the glucose-binding protein ttGBP from *Thermus thermophilus*. The initial sensor was further optimized by linker mutagenesis, and site directed mutagenesis was used to produce a series of affinity mutants. MGlucoMeter2.6-1 m with an affinity of 1 mM for glucose was then used to monitor the accumulation of glucose in Arabidopsis roots as well as the accumulation and transport of glucose in Arabidopsis seedling roots after supply of sucrose to shoots.

RESULTS AND DISCUSSION

Development of ultrasensitive matryoshka-type glucose sensors

Proteins from thermophiles often exhibit enhanced stability. For generating a Matryoshka-type glucose sensor, the glucose-binding protein from *Thermus thermophilus*, for which crystal structure information is available, was chosen as the recognition element (Cuneo et al., 2009; Keller et al., 2021) (Figures S1 and S2). The glucose-binding protein ttGBP had previously been used to develop the intensiometric glucose sensor iGlucoSnFR. iGlucoSnFR was generated by inserting the circularly permutated cpGFP into ttGBP, without the leader peptide, between residues 326 and 327, using a linker combination of left linker Pro-Ala (L1-PA) and right linker Asn-Pro (L2-NP) (Keller et al., 2021, Text S1). Analogous to the construction of iGlucoSnFR, here a Matryoshka cassette consisting of the superfolder cpsfGFP variant carrying an insertion of the Large Stokes Shift (LSS) mApple (LSSmApple) that had been used to generate MatryoshCaMP6s (Ejike et al., 2024) was inserted into ttGBP without the N-terminal leader sequence to generate MGlucoMeter1.0 (https://www.molecular-physiology.hhu.de/en/resources-1/mglucometer-10). The nested large stokes shift fluorophore provides a reference fluorophore for ratiometric imaging. The linkers that flank the fusion site between cpsfGFP and the recognition element had been shown to be important for excited-state proton transfer (ESPT) (De Michele et al., 2013). The initial MGlucoMeter1.0 sensor also had only limited sensitivity. To further increase the sensitivity and detection range for *in vivo* measurements, the codons for amino acid pairs in the linker sequence flanking the Matryoshka cassette in MGlucoMeter1.0 were mutated. An alanine scan corresponding to 19 amino acids surrounding the cpsfGFP insertion site was performed; that is, the hinge region of the glucose-binding domain, and artificial linker sequences (FNNPNAYGQSAM/DSDPSKYPASH); (Figure 1a, Table 1). A set of 32 mutants carrying single, double or triple alanine replacements were characterized in more detail (Table 1). Fluorometric analysis of the glucose-induced ratio changes of the series indicated that some of the sensors lost responses to glucose addition, some showed altered affinities, and some were improved (Figure 1b). We chose the variant MGlucoMeter2.6 with the highest sensitivity ($\Delta F/F_0$ 3.0) for generating a series of affinity variants.

Generation of an affinity variants for MGlucoMeter2.6

Previous studies had shown that the glucose sensor FLIPglu600μ with an affinity for glucose of 600 μM was well suited for recording glucose responses in Arabidopsis roots. We here generated a series of affinity mutants of MGlucoMeter2.6 by site directed mutagenesis of candidate residues that interact with the glucose molecule, that is, H66 and H348 (numbering based on the previously published sequence of ttGBP) (Figure S1; Text S1 and S2) (Chaudhuri et al., 2008; Cuneo et al., 2009; Keller et al., 2021). The resulting mutants exhibited affinities (K_d) for glucose of approximately 355 nM, 717 μM, 1 mM, and 7.3 mM, respectively

Figure 1. *In vitro* screening of MGlucoMeter variants with increased sensitivity.
(a) Construct map of MGlucoMeter2.6 carrying an insertion of the Green-Apple cassette (GA; cpsfGFP-LSSmApple) in ttGBP. The amino acid residues substituted for MGlucoMeter are indicated as underlined. Four amino acid linker sequences connecting the Green-Apple cassette and ttGBP are indicated with blue underline. An Alphafold prediction for the sensor is shown in Figure S2.
(b) The fluorescence responses of 32 purified MGlucoMeter variants, generated by the alanine scan, were tested *in vitro* for changes upon addition of 10 mM glucose.

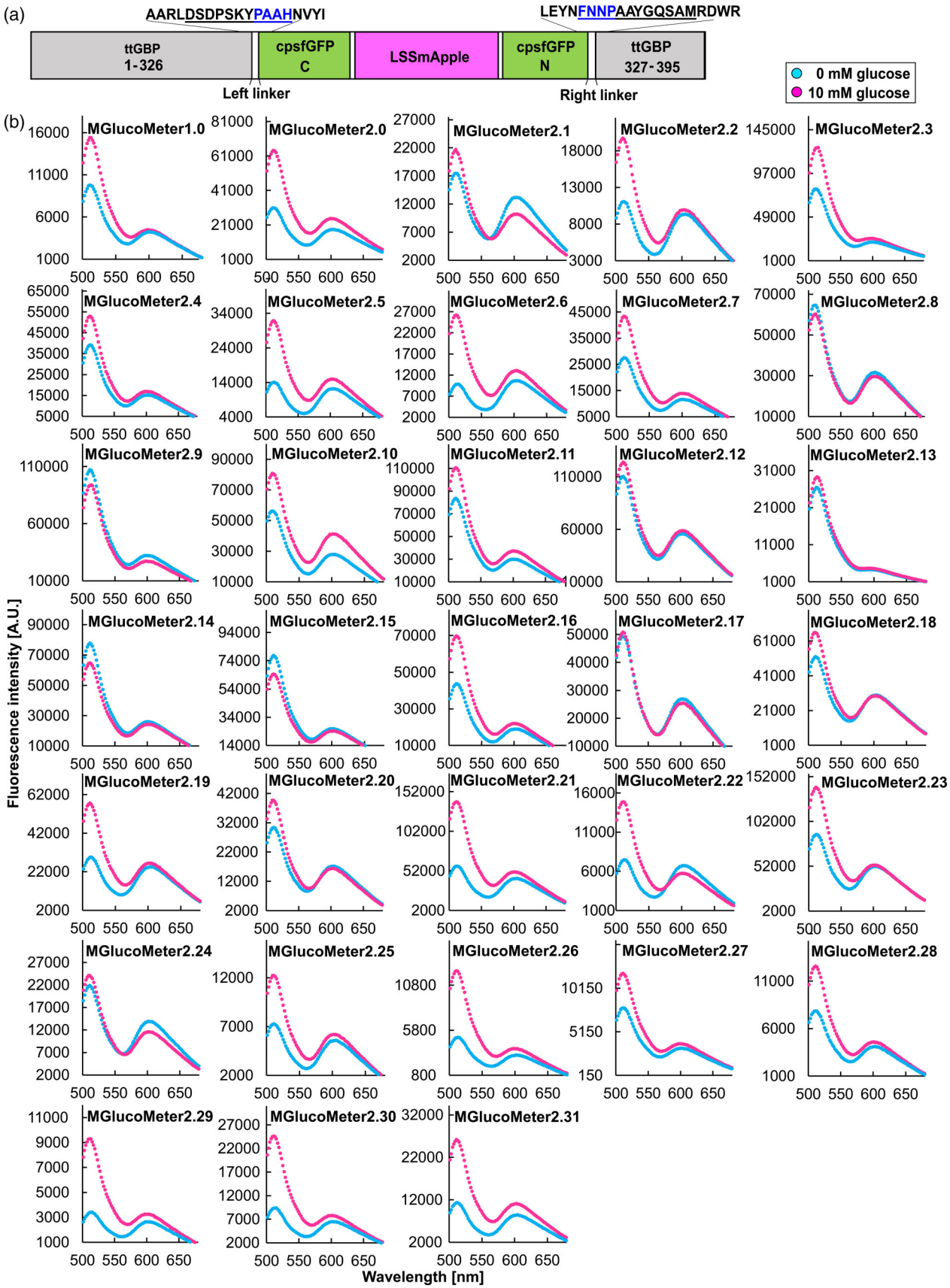

The Plant Journal published by Society for Experimental Biology and John Wiley & Sons Ltd.,
The Plant Journal, (2026), **125**, e70778

Table 1 Sequence of linker/hinge sequence subjected to alanine scanning of MGlucoMeter variants

MGlucoMeter	$\Delta F/F_0$	Left linker	Right linker
MGlucoMeter1.0	0.50	DSDPSKYPASH	FNNPNAYGQSAM
MGlucoMeter2.0	0.84	DSDPSKYPASH	FANPNAYGQSAM
MGlucoMeter2.1	0.24	DSDPSKYPASH	FNNPNAAGQSAM
MGlucoMeter2.2	0.85	DSDPSKYPAAH	FNNPNAYGQSAM
MGlucoMeter2.3	0.50	DSDPSKYPASA	FANPNAYGQSAM
MGlucoMeter2.4	0.36	DSDPSKYPAAH	ANNPNAYGQSAM
MGlucoMeter2.5	1.1	DSDPSKYPAAH	FANPNAYGQSAM
MGlucoMeter2.6	**3.00**	DSDPSKY**PA**A**H**	**FNNP**AAYGQSAM
MGlucoMeter2.7	0.45	DSDPSKYAASH	ANNPNAYGQSAM
MGlucoMeter2.8	<0	DSDPSKYPASH	FNAPNAYGQSAM
MGlucoMeter2.9	<0	DSDPSKAPASH	FNNPNAYGQSAM
MGlucoMeter2.10	0.44	DSDPSAYPASH	FNNPNAYGQSAM
MGlucoMeter2.11	0.32	DSDPSKYPASA	FNAPNAYGQSAM
MGlucoMeter2.12	0.13	DSDPSKYPASA	FNNANAYGQSAM
MGlucoMeter2.13	0.10	DSDPSKYAASH	FANPNAYGQSAM
MGlucoMeter2.14	<0	DSDPSKYAASH	FNAPNAYGQSAM
MGlucoMeter2.15	0.59	DSDPSKYAASH	FNNANAYGQSAM
MGlucoMeter2.16	0.46	DSDPSKYAASH	FNNPAAYGQSAM
MGlucoMeter2.17	0.03	DSDPSKYPAAH	FNNPNAYGQSAA
MGlucoMeter2.18	0.27	ASDPSKYPAAH	FNNPAAYGQSAM
MGlucoMeter2.19	0.95	DADPSKYPAAH	FNNPAAYGQSAM
MGlucoMeter2.20	0.31	DADPSKYPAAH	FNNPNAYGQSAM
MGlucoMeter2.21	1.39	DSDASKYPASH	FNNPAAYGQSAM
MGlucoMeter2.22	1.00	DSDPSKYPAAH	FNNPAAYGQAAM
MGlucoMeter2.23	0.61	DSDPAKYPASH	FNNPAAAGQSAM
MGlucoMeter2.24	0.10	DSDPSKYPASH	FANPAAYGQSAM
MGlucoMeter2.25	0.68	DSDPSKYPAAH	FNNPAAAGQSAM
MGlucoMeter2.26	1.49	DSDPSKYPAAH	FNNPAAYAQSAM
MGlucoMeter2.27	0.50	DSDPSKYPAAH	FNNPAAYGASAM
MGlucoMeter2.28	0.59	DSDPSKYPAAH	FNNPAAYGQSAA
MGlucoMeter2.29	1.74	DSDASKYPAAH	FNNPAAYGQSAM
MGlucoMeter2.30	1.63	DSDPAKYPAAH	FNNPAAYGQSAM
MGlucoMeter2.31	1.05	DSDPSKYPASH	FNNPAAYGQSAM

Bold indicates sensor chosen for further studies. Yellow highlight: alanine mutation in linker region relative to MGlucoMeter1.0. The underline is meant to separate MGlucoMeter 1.0, the strating sensor used here from the new variants.

(Figures 2 and 3 and Table 2). All affinity variants showed higher sensitivity ($\Delta F/F_0$ 1.90–3.69) compared to the original FLIPglu (Δr_{max} 0.29) (Figure 3, Table 3) (Fehr et al., 2003). Notably, the detection range of the MGlucometer2.6 sensors is substantially larger compared to FLIPglu, which covered less than two orders of magnitude (Table 3) (FLIPglu-600 μ: 65.4–5301 μM) (Fehr et al., 2003). Analysis of the substrate specificity showed that glucose had the highest affinity followed by galactose, whereas other sugars showed much lower affinities (Figure 4, Table 4). Of note, MGlucoMeter2.6-1 m used below for *in planta* analyses, did not show detectable *in vitro* responses to the addition of sucrose and is thus suitable for specifically monitoring glucose levels or changes (Figure 4). The principle of genetically encoded sensors is based on the translation of a conformational rearrangement of a binding protein into a fluorescent output. However, other factors such as ionic strength or pH affect protein conformation as well as the fluorophores. *In vitro* titration of the MGlucoMeter2.6 series showed a trend for a correlation of increased ratios with increasing pH over a range of 4.3 to 8 (Figure S3). Previous studies used FLIPglu affinity mutants to evaluate whether the sensor response was caused by glucose addition to roots or by changes in other parameters such as pH (Chaudhuri et al., 2008). If the observed change were caused by changes in other parameters, such as cytosolic pH, affinity variants are expected to show comparable responses despite different detection ranges for glucose; whereas if the change were due to changes in glucose levels, different concentration-dependent responses are expected. We thus surmise that the affinity mutants MGlucoMeter2.6-353n, 15 μ, 7 m may be useful for distinguishing between treatment-induced pH or cytosolic glucose changes *in vivo* experiments.

Monitoring uptake of glucose into Arabidopsis roots

In a previous study, fluorescence from an earlier version of FLIPglu glucose sensors in stably transformed Arabidopsis plants was obtained only in the *rdr6* RNA silencing mutant background, most likely due to gene silencing (Deuschle et al., 2006). Consistently, in the Col-0 background, here, transformants of Col-0 wild type did not show substantial fluorescence in the roots of MGlucoMeter2.6 expressing Arabidopsis. To be able to monitor glucose concentration changes *in planta*, MGlucoMeter2.6-1 m was expressed from the *UBQ10* promoter in the cytosol of the Arabidopsis gene-silencing mutant *rdr6*. *Roots* of 10-day-old seedlings mounted in a hand-made perfusion chamber were perfused with square pulses of glucose, and the emission change after the addition of glucose was monitored under an inverted fluorescence microscope. Within 1 min after the addition of 1 mM glucose, MGlucoMeter2.6-1 m showed a detectable emission ratio change in the root (Figure 5a–d, Figures S4 and S5, Video S1). Within about 2 min, the maximal response was reached, which would correspond to reaching the K_d of 1 mM, similar as in previous experiments with FRET glucose sensors which had shown that extra- and intracellular levels of glucose rapidly equilibrated (Chaudhuri et al., 2008). During further perfusion, the sensor response remained constant and declined rapidly after replacing glucose-containing buffer with glucose-free buffer, consistent with the reversibility of the response.

Detection of glucose accumulation in roots after by sucrose supply to leaves

Sucrose generated by photosynthesis is loaded into the phloem of leaves and translocated from shoot to root. Sucrose utilization requires metabolic activities, for example, invertases, that produce glucose and fructose. To investigate whether the MGlucoMeter2.6 can detect the production of glucose in roots that is derived from sucrose delivered by long-distance translocation from the shoots, shoots of

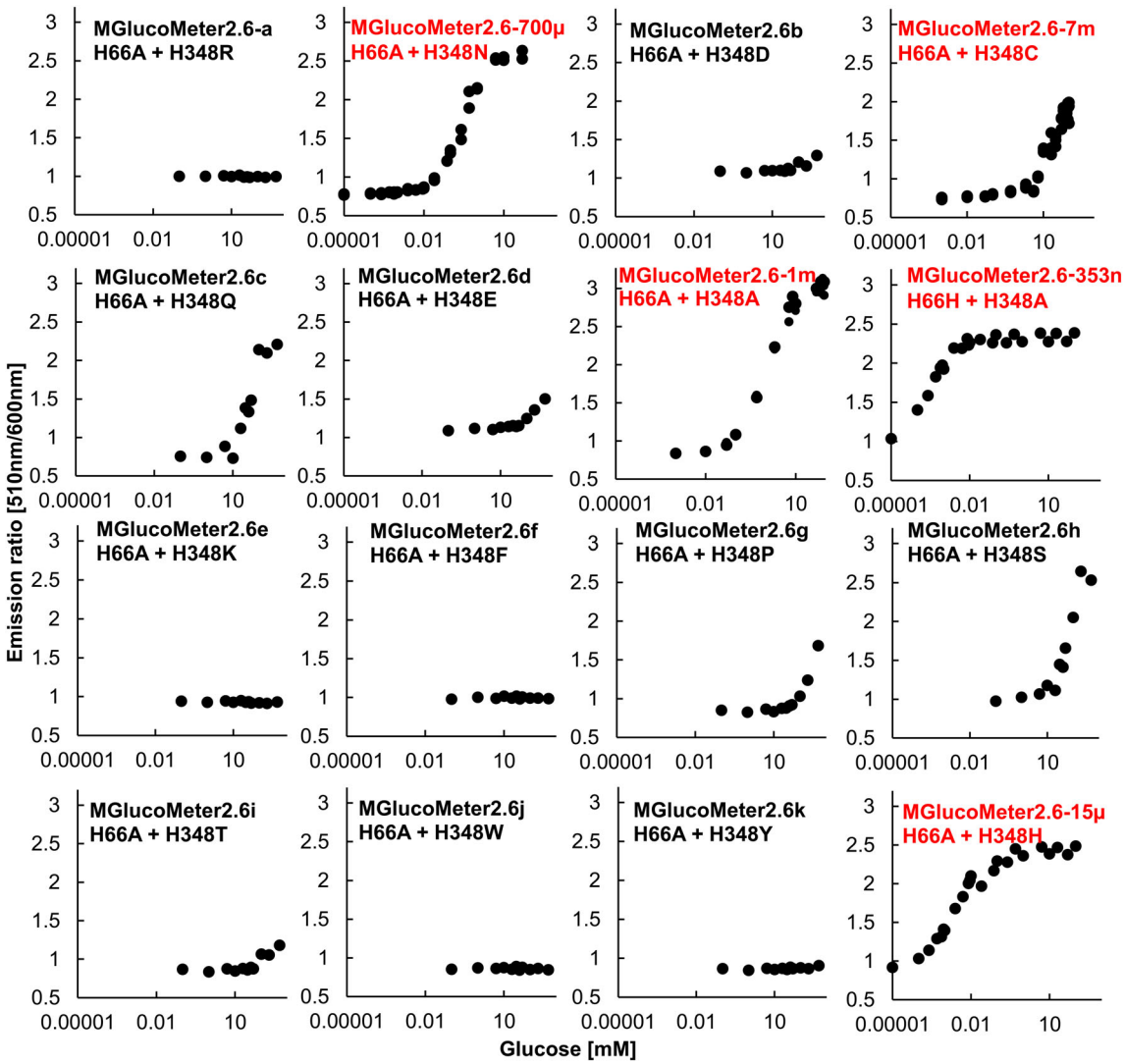

Figure 2. *In vitro* screening of affinity variants based on MGlucoMeter2.6.
16 affinity variants, generated by site directed mutagenesis at H66 and H348, were characterized *in vitro* using the cpsfGFP/LSSmApple emission ratio. Purified protein was titrated with increasing glucose concentrations. Sensors marked in red are chosen for further studies.

Arabidopsis plants expressing MGlucoMeter2.6-1 m were exposed to media containing sucrose, and glucose accumulation was monitored in root tips (Figure 6b). About 40 min after sucrose supply to the shoots, a ratio change was detected in roots, indicating that sucrose had been translocated from the shoot to the root tip unloading zone, where sucrose was then converted to glucose (Figure 6, Figures S7 and S8, Video S2). No response was observed in epidermal cells outside the unloading zone, making it unlikely that sucrose traveled on the plant surface from shoot to root (Figure S8). As one may expect, we did not observe a change in glucose levels in the vasculature, consistent with delivery of sucrose from the shoot in the phloem, followed by unloading in the unloading zone in the root and hydrolysis and diffusion in the unloading zone (Figure S9). Of note, *in vitro*, MGlucoMeter2.6-1 m did not show detectable responses even to high sucrose concentrations (Figure 4). These observations are consistent with the important role of cytosolic invertases CINV1 and 2 for root growth and development (Barratt et al., 2009). In particular, CINV1 mRNA levels were high in cells in the unloading zone (Figure S10). Thus, detection of glucose accumulation by sucrose treatment to shoot confirmed that the sensitivity ($\Delta R/R_0$ 180–230%) of MGlucoMeter2.6-1 m is high enough for effective and sensitive wide-view imaging to explore long-distance sugar translocation and metabolism in Arabidopsis.

In summary, we developed a new series of genetically encoded ultrasensitive ratiometric glucose sensors using the Matryoshka concept, in which excitation at a single wavelength enables detection of the emission for the

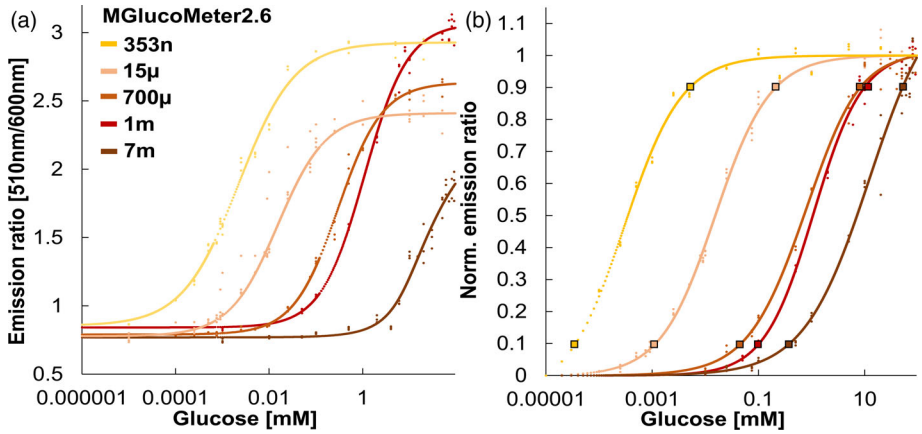

Figure 3. Glucose concentration-dependent changes in fluorescence emission ratio of MGlucoMeter2.6 affinity variants.
(a) *In vitro* substrate titrations of MGlucoMeter2.6 affinity variants. MGlucoMeter2.6-353n (H66H + H348A), MGlucoMeter2.6-15 µ (H66A + H348H), MGlucoMeter2.6-700 µ (H66A + H348N), MGlucoMeter2.6-1 m (H66A + H348A), and MGlucoMeter2.6-7 m (H66A + H348C) were generated by site directed mutagenesis. The *in vitro* properties of each sensor are summarized in Tables 2 and 3. The mean of three technical replicates is plotted. Experiments were repeated independently two times with comparable results.
(b) Estimation of the detection range of MGlucoMeter2.6 (linear range between 10 and 90% saturation).

Table 2 Affinity and mutation of MGlucoMeter2.6 variants

MGlucoMeter	Mutation	K_d glucose
MGlucoMeter2.6a	H66A + H348R	n.r.
MGlucoMeter2.6-700 µ	**H66A + H348N**	**717 ± 0.5 µM**
MGlucoMeter2.6b	H66A + H348D	n.r.
MGlucoMeter2.6-7 m	**H66A + H348C**	**7.3 ± 0.5 mM**
MGlucoMeter2.6c	H66A + H348Q	42.9 mM
MGlucoMeter2.6d	H66A + H348E	>150 mM
MGlucoMeter2.6-1 m	**H66A + H348A**	**1 ± 0.01 mM**
MGlucoMeter2.6-353n	**H66H + H348A**	**355 ± 2.7 nM**
MGlucoMeter2.6e	H66A + H348K	n.r.
MGlucoMeter2.6f	H66A + H348F	n.r.
MGlucoMeter2.6 g	H66A + H348P	210.5 mM
MGlucoMeter2.6 h	H66A + H348S	65.1 mM
MGlucoMeter2.6i	H66A + H348T	95.3 mM
MGlucoMeter2.6j	H66A + H348W	n.r.
MGlucoMeter2.6 k	H66A + H348Y	n.r.
MGlucoMeter2.6-15 µ	**H66A + H348H**	**15 ± 0.46 µM**

Bold indicates sensor variant chosen for further studies.
n.r., no response.

Table 3 Sensitivity and detection range of MGlucoMeter2.6 variants

MGlucoMeter	$\Delta F/F_0$	Detection range (10 ~ 90% sat)
MGlucoMeter2.6-353n	1.90 ± 0.06	0.04 µM ~ 5.1 ± 0.1 µM
MGlucoMeter2.6-15 µ	3.00 ± 0.13	1.1 ± 0.005 µM ~ 216 ± 14.4 µM
MGlucoMeter2.6-700 µ	2.63 ± 0.18	46.6 ± 1.6 µM ~ 8.6 ± 1.0 mM
MGlucoMeter2.6-1 m	**3.69 ± 0.14**	**102.7 ± 0.003 µM ~ 10.0 ± 0.76 mM**
MGlucoMeter2.6-7 m	2.21 ± 0.19	0.39 ± 0.03 mM ~ 55.9 ± 11.4 mM

Bold indicates sensor variant chosen for further studies.

sensory domain, a circularly permutated superfolder GFP and the large stokes shift reference fluorophore LSSmApple. The sensory domain was a periplasmic glucose-binding protein from a thermophile, which is likely more robust to insertion and mutagenesis. An alanine scan yielded sensors with a high sensitivity. We generated affinity mutants and used the optimized MGlucoMeter2.6 with an affinity for glucose of 1 mM to monitor glucose accumulation in intact Arabidopsis roots either from externally added glucose to roots or from hydrolysis of sucrose delivered from the shoot. Rapid hydrolysis of sucrose had previously been detected with a FRET glucose sensor (Chaudhuri et al., 2008).

Here we obtained evidence that sucrose is likely hydrolyzed after release from the phloem upon delivery from the shoot via the phloem. Cell-to-cell movement in the root is most likely mediated by plasmodesmata (Chaudhuri et al., 2008; Stadler et al., 2005; Wright & Oparka, 1997). The new sensors can likely be deployed in a wide range of organisms, as previously shown for the FRET glucose sensors, including bacteria, yeast, and human cell lines (Bermejo et al., 2010; Bermejo et al., 2013; Bermejo, Haerizadeh, et al., 2011; Fehr et al., 2005; Takanaga et al., 2008).

MATERIAL AND METHODS

Construction of MGlucoMeter

MGlucoMeter2.0 were generated from the initial construct MGlucoMeter1.0 (www.molecular-physiology.hhu.de/en/resources-1/mglucometer-10), which carries an insertion of the cpsfGFP-LSSmApple cassette from GA-MatryoshCaMP6s in the hinge region

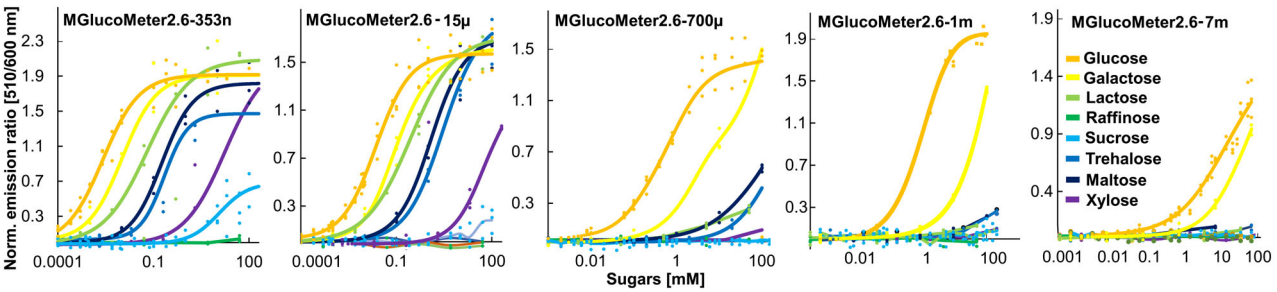

Figure 4. *In vitro* determination of the substrate selectivity of MGlucoMeter2.6 affinity variants.
In vitro substrate titrations of MGlucoMeter2.6 affinity variants. MGlucoMeter2.6-353n, MGlucoMeter2.6-15 µ, MGlucoMeter2.6-700 µ, MGlucoMeter2.6-1 m, MGlucoMeter2.6-7 m were tested to determine the substrate selectivity. The *in vitro* properties of each sensor are summarized in Table 4. The mean of three technical replicates is plotted. Experiments were repeated independently two times with comparable results.

Table 4 Substrate selectivity of MGlucoMeter2.6 variants

	MGlucoMeter2.6				
K_d sugars	353n	15 µ	700 µ	1 m	7 m
Glucose	355 ± 2.7 nM	15 ± 0.4 µM	717 ± 0.5 µM	**1 ± 0.01** mM	7.3 ± 0.5 mM
Xylose	1.83 ± 0.6 mM	25.6 ± 2.3 mM	n.r.	**n.r.**	n.r.
Maltose	62.3 ± 0.07 µM	0.97 ± 0.02 mM	n.r.	**n.r.**	n.r.
Trehalose	0.23 ± 0.06 mM	0.72 ± 0.02 mM	n.r.	**n.r.**	n.r.
Sucrose	n.r.	n.r.	n.r.	**n.r.**	n.r.
Raffinose	n.r.	n.r.	n.r.	**n.r.**	n.r.
Lactose	11 ± 2.2 µM	n.r.	n.r.	**n.r.**	n.r.
Galactose	2.8 ± 0.3 µM	38.2 ± 4.5 µM	2.87 ± 0.2 mM	**14.9 ± 0.7** mM	25.5 ± 2.2 mM

Bold indicates sensor variant chosen for further studies.
n.r. no response.

of ttGBP from *Thermus thermophilus* in the pRSETb T7 expression vector (Thermo Scientific, Waltham, MA, USA; V35120) (Cuneo et al., 2009; Ejike et al., 2024) (Figure 1a, Table 1). An Alphafold model of the sensor is shown in Figure S2. The expressed gene product (P0328) of ttGBP lacks the 21-bp leader sequence (Cuneo et al., 2009). An alanine scan of the linker and hinge region (amino acids targeted left linker/hinge region: DSDPSKYPASH; right linker/hinge region FNNPNAYGQSAM) was performed by inverse PCR (Figure 1a, Table 1). PCR products were amplified using PrimeSTAR GXL (Takara Bio; R050B) (Table S1). The resulting product was cleaned up by gel extraction using the NucleoSpin column kit (Macherey-Nagel, Düren, Germany; 740 609). Affinity variants were generated by introducing individual point mutations into ttGBP. All constructs were validated by DNA sequencing (Microsynth SEQLAB, Göttingen, Germany). Plasmids containing the MGlucometer2.6 affinity variants are available from AddGene (www.addgene.org).

Expression and purification of the MGlucoMeter

E. coli BL21 (DE3) [*fhuA2 [lon] ompT gal (λ DE3) [dcm] ΔhsdS; λ DE3 = λ sBamHIo ΔEcoRI-B int::(lacI::PlacUV5::T7 gene1) i21 Δnin5*] (New England Biolabs, Ipswich, MA, USA; C2527I) was transformed with pRSETb containing MGlucoMeter plasmids. Single colonies were inoculated into 3 ml of LB medium (Duchefa Biochemie, Haarlem, Netherlands; 4800-94-6) containing 50 µg/ml carbenicillin (Sigma-Aldrich, St. Louis, MU, USA; C1389) in glass tubes (Hardy diagnostics, Santa Maria, CA, USA; 1517) sealed with ϕ15/16 mm silver aluminum caps (Lüdi, Regensdorf, Switzerland; LUDI184010631) and incubated at 37°C with shaking at 200 rpm for 14–18 h. 2 ml of the starter culture were transferred into 100 ml LB medium containing 50 µg/ml carbenicillin disodium, 0.2% D-lactose (Sigma-Aldrich; 64 044–51-5), and 0.05% D-glucose monohydrate (Thermo Scientific Chemicals; 14 431–43-7) in 500 ml Erlenmeyer flasks without baffles sealed with ϕ37/39 mm silver screw caps (Carl Roth selection, Karlsruhe, Germany; K395.1). After 2 h of incubation at 37°C with shaking at 200 rpm, cultures were transferred to 20°C incubator with shaking at 200 rpm and incubated for 48 h. Bacterial cultures were cooled on ice and centrifuged at 3790 × ***g*** for 10 min at 4°C. The cell sediment was stored at −20°C for at least 14 h to increase the potential for protein folding in vivo. After thawing on ice, the sediment was resuspended in 1.5 ml 20 mM MOPS (Roth; 1132-61-2), pH 7.0. To prevent sensor degradation, one cOmpleteTM ULTRA Tablet Mini protease inhibitor cocktail (Merck, Darmstadt, Germany; 1 183 670 001) was added per 100 ml of all purification buffers. Cells were lysed by sonication at 50 amplitudes (QSonica Q700 Sonicator, Newtown, CT, USA), with a total processing time of 45 s (3 s pulse on, 8 s pulse off). The sonicated sample was centrifuged at 15871 × ***g*** for 10 min at 4°C to remove cellular debris. His-tagged MGlucoMeter sensor proteins were purified using Ni-NTA agarose beads (Qiagen, Hilden, Germany; 30 210). Prior to lysate application, 1.5 ml Ni-NTA agarose beads were loaded onto an affinity column and washed with 10 ml of 20 mM MOPS, pH 7.0. After the loading of the lysate, the column was washed again with 10 ml of 20 mM MOPS, pH7.0. His-tagged MGlucoMeter protein was eluted with 1.5 ml of 250 mM imidazole (Sigma-Aldrich; 1467-16-9) and 20 mM MOPS, pH 7.0. Protein concentration was determined by a NanoDrop One (Thermo Scientific). Purified sensors were incubated at 4°C for at least 14 h to ensure maturation of the fluorescent protein.

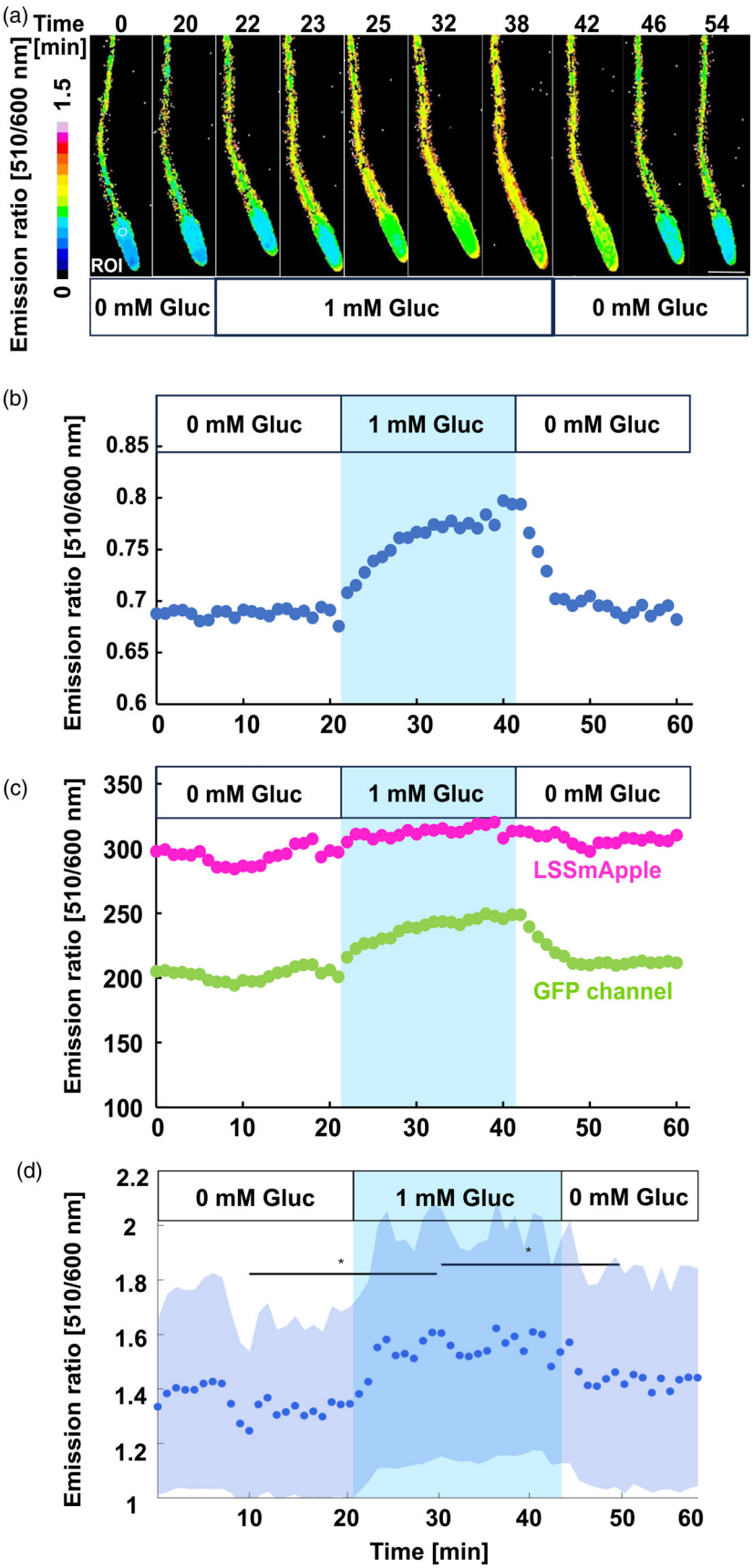

Figure 5. Time-dependent accumulation of glucose in Arabidopsis roots monitored with MGlucoMeter2.6-1 m in response to perfusion of roots with glucose.
(a) Data from 10-day-old seedlings expressing MGlucoMeter2.6-1 m (Video S1). Maximum intensity Z-projection images for the emission ratio of cpsfGFP over LSSmApple. Scale bar: 200 μm.
(b) Quantification of the time-dependent *in vivo* response of MGlucoMeter2.6-1 m in Arabidopsis roots for the ROI: white circle in Figure 5a. The cpsfGFP/LSSmApple emission ratio was plotted. Blue square indicates square pulse of 1 mM glucose-containing medium.
(c) Fluorescence changes in the individual channels (cpsfGFP and LSSmApple) emission, in response to glucose. The experiment was repeated with three biological replicates (individual roots) and three times independently with comparable results (Figures S4 and S5).
(d) Emission ratio changes were analyzed using a linear mixed-effects model. Treatment with 1 mM glucose significantly increased the emission ratio compared to no glucose. Asterisk (*) indicates statistical significance at $p < 0.01$.

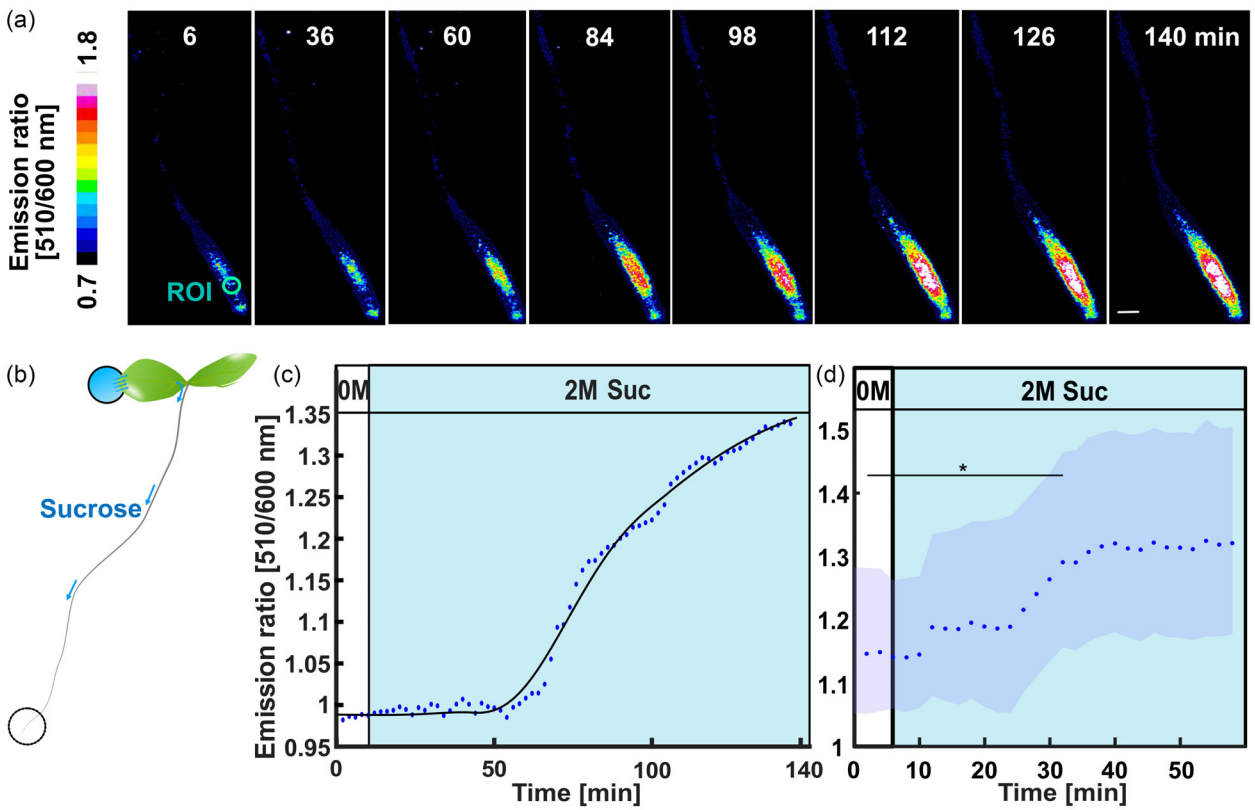

Figure 6. Detection of glucose accumulation in root tips of MGlucoMeter2.6-1 m expressing Arabidopsis seedlings in response to sucrose application to the cotyledons.
(a) Data from 12-day-old seedlings expressing MGlucoMeter2.6-1 m (Video S2). Maximum intensity Z-projection and emission ratio of cpsfGFP over LSSmApple. Scale bars: 100 μm. ROI used for quantification of the emission ratio in Figure 6b is shown as a blue circle.
(b) Experimental setup for observing glucose accumulation in root tips. ROI used for quantification of the emission ratio in Figure 6c and fluorescence intensity of individual channels in Figure S5 are shown as dotted black circles. The tip of one of the cotyledons was exposed to 2 M sucrose in ½ salt strength MS medium. The seedlings used for experiment were at the two-leaf stage (cotyledons plus the first true leaves). Roots were placed on 1% agar plates containing ½ salt strength MS.
(c) Time-dependent *in vivo* glucose accumulation in Arabidopsis roots after exposure of the cotyledons to sucrose. Emission ratio of cpsfGFP over LSSmApple was plotted. Blue square indicates treatment with 2 M sucrose-containing medium of MGlucometer2.6-1 m expressing Arabidopsis cotyledons. The experiment was repeated with three biological replicates (individual roots) and three times independently with comparable results (Figures S7 and S8). Emission ratios at each time point were imported from an Excel file and smoothed using the LOESS method.
(d) Emission ratio changes were analyzed using a linear mixed-effects model. Treatment with 2 M sucrose significantly increased the emission ratio compared no sucrose. Asterisk (*) indicates statistical significance at $p < 0.01$.

Fluorimetric analysis of MGlucoMeter2.0 sensors

For each well, 10 μl of purified sensor solution was mixed with 190 μl 20 mM MOPS (pH 7.0). Ligand titrations were performed using a TECAN Spark microplate reader (Tecan Austria GmbH, Männedorf, Switzerland; 704 004 367). Steady-state fluorescence spectra were recorded with excitation wavelength at 453 ± 20 nm and emission spectra from 499 to 700 nm in 2 nm steps. Measurements were recorded in the top-reading mode with a gain of 80–130 and the temperature controlled at 27 ± 0.5°C. Spectra were background-subtracted agianst wells containing 20 mM MOPS (pH 7.0). Analyses were performed in 96-well clear, flat-bottom,

microplates (Corning, Berlin, Germany; 3370). Fluorescence emission ratios were calculated as cpsfGFP emission intensity (λ_{ex} 480 nm, λ_{em} 515 nm) divided by LSSmApple emission intensity (λ_{ex} 460 nm, λ_{em} 600 nm). The baseline ratio defined as R_0 and the ratio at increasing ligand concentrations as R. Data were normalized accordingly;

$$\Delta R/R_0 = (R - R_0)/R_0$$

Data analyses and visualization were performed using Excel, Origin Lab 2020, and Affinity Designer. Sigmoid curve fitting was performed with MyCurveFit (https://mycurvefit.com). Values are reported as the mean ± standard error of $\Delta R/R_0$ or $\Delta F/F_0$ from n = 3 biological replicates ($n = 3$ technical replicates per biological replicates) out of two independent titrations. The dissociation constant (K_d) was defined as the ligand concentration at 50% $\Delta R_{max}/R_0$ in the fitted sigmoid function.

Cloning of MGlucometer2.6 constructs for expression in plants

MGlucometer2.6-1 m was subcloned into pAY367-HTv443-UBQ10-Hspt binary vector (provided by Dr. A. Yoshinari, Institute for Transformative Biomolecules, ITbM, Nagoya University, Nagoya, Japan), which contains the Arabidopsis UBQ10 promoter and Hsp18.2 terminator. To insert MGlucometer2.6-1 m, pAY367-HTv443-UBQ10-Hspt was digested with *AscI* and *ApaI* restriction enzymes. Ligation reaction was carried out in the solution mixture containing 40 fmol DNA of the entry clones, 1× T4 DNA ligase buffer (Thermo Fisher, Waltham, MA, USA; B69) and 5 U T4 DNA ligase (Thermo Fisher; EL0012) in a total volume of 20 µl (Thermocycler, Biorad T100, Hercules, CA, USA: 22°C for 10 min). The Arabidopsis gene-silencing mutant *rdr6-11* (Deuschle et al., 2006; Peragine et al., 2004) was transformed using the floral dip method. Transformed plants were selected on 50 µg/ml kanamycin and 2.35 mM MES containing ½ salt strength Murashige and Skoog (MS) medium (Duchefa Biochemie; M0255), adjusted to pH 5.7 with KOH, and solidified with 1% agar (Merck; 05040).

Plant growth conditions

MGlucoMeter2.6-1 m expressing Arabidopsis seeds were surface sterilized with 75% ethanol containing 0.08% Tween20, sown on ½ salt strength Murashige Skoog medium (Duchefa Biochemie; M0255; half the concentration of MS salts relative to supplier recipe) containing 2.35 mM MES, adjusted to pH 5.7 with KOH, and solidified with 1% agar (without addition of sugars). Plants were sealed with micropore tape and vernalized at 4°C for 1 day. Plants were grown at 22°C for 5 days after germination under the long day conditions (16 h light/8 h dark, light intensity was 110 µmol m^{-2} s^{-1}).

Root uptake kinetics measured with an automated perfusion system

MGlucoMeter2.6 seedlings were germinated, and 10-day-old seedlings were transferred to ½ salt strength MS medium in a 60 µ-Dish (v; 81 158) and immobilized using double sided adhesive tape (Tesa Tape, Beiersdorf AG, Norderstedt, Germany; 05338). Seedlings were acclimated for 20 min by perfusion with mock buffer (¼ salt strength MS containing 2.35 mM MES, pH 5.7, no sugars added) in the recording room. A peristaltic pump was used (Fisher Scientific, Hampton, NH, USA; Cytiva 18-1110-91, flow rate; 2 ml/min) to perfuse the filtered ¼ salt strength MS containing 2.35 mM MES (pH 5.7) liquid media to the whole seedling. Fully automated buffer exchange to 1 mM glucose containing ¼ salt strength MS containing 2.35 mM MES (pH 5.7) liquid media was achieved using a valve controller (Automate scientific, Berkeley, CA, USA; ValveBank Controllers). The dead volume (delayed arrival of buffer in a fluid reservoir) was assessed in the perfusion setup using a fluorescent dye (ATTO 390; ATTO-TEC GmbH, Siegen, Germany; AD 390–25). The delay was calculated by taking the saturated fluorescence intensity as 100% and determining the time required to reach 85% or 15% of that fluorescence intensity. An Olympus IXplore SpinSR spinning disk confocal microscope was used for imaging. Samples were excited with a 488 nm laser (Obis; 100 mW, used at 10–30% power). The microscope was equipped with a Yokogawa confocal scanning unit (CSU)-W1 SoRa micro-lensed pinhole disk and an Olympus UAPON 10× UPL SAPO10×2 (Olympus, Hamburg, Germany). Emission intensities were collected in sequential stacks using a 525/50 nm emission filter for GFP, 617/73 nm emission filter for LSSmApple. For detection, an Andor iXon Ultra 888 electron-multiplying charge coupled device (EMCCD) (Oxford Industries, Wiesbaden, Germany) was used. Z-stacks were set by using a Mad City Labs Z-axis piezo nano positioner with 300 nm travel range (OLY-S1023-Nano-ZL300-OSSU, Mad City Labs, Madison, WI, USA). Full Z-stack acquisitions for each channel were performed at a frame rate of 1 min. The exposure time for each channel was 50 msec, with 4 × 4-pixel binning.

Quantitative imaging of glucose in roots in response to sucrose addition to shoots

Seedlings were acclimated for at least 2 h on 1% agar plates containing ½ salt strength MS and 2.35 mM MES (pH 5.7), sealed with micropore tape, in the recording room. Seedlings were placed on 1% agar plates containing ½ salt strength MS and 2.35 mM MES (pH 5.7) in a glass bottom chamber (Ibidi, Gräfelfink, Germany; µ-slide 1 well glass bottom). A flat PCR tube cap filled with 2 M sucrose in ¼ salt strength MS containing 2.35 mM MES (pH 5.7) liquid media was placed in the glass bottom chamber, with the tip of cotyledon submerged in the sucrose solution (Figure 6b). Quantitative glucose imaging was performed using a Zeiss AxioZoom V16 zoom microscope equipped with a X-Cite XYLIS LED Illumination System (XT720L), a 1× objective lens (PlanNeoFluar Z 1×/0.25 NA, FWD 56 mm; Zeiss, Oberkochen, Germany), and a Hamamatsu ORCA Flash4.0 CMOS camera. Zoom magnification was set between 7× and 10×, and pixel binning was set to 2 × 2 or 4 × 4-pixel binning for acquisitions. cpsfGFP fluorescence was detected using a filter cube with a 488/10 nm excitation filter, a 491 nm long-pass dichroic mirror, and a 519/26 nm emission filter. LSSmApple fluorescence was detected using a filter cube with a 488/10 nm excitation filter, a 514 nm long-pass dichroic mirror, and a 605/50 nm emission filter. A motorized *xy* stage (Zeiss) was used for time-lapse tiling acquisitions. Tiles were stitched using ZEN Blue 2.6 software (Zeiss). *Z*-step sizes were set equal to the optical section thickness (2–4 µm).

Image analyses

Segmentation and labelling were performed with the FRETENATOR plugins in Fiji (Schindelin et al., 2012). Segmentation settings were optimized for each experiment. The GFP channel was used for segmentation. A watershed algorithm was used for the image segmentation. Difference of Gaussian kernel size was determined empirically due to different magnifications, resolutions and amount of noise. As a default, Otsu thresholds were used for segmentation in FRETENATOR (Rowe et al., 2022). For image analysis, curve fitting was performed using the LOESS method (smooth function) (Cleveland & Devlin, 1988) in MATLAB R2025a. (https://www.mathworks.com/products/new_products/release2023a.html).

A smoothing span of 0.25 was used, and the span was adjusted interactively using a MATLAB slider to determine the optimal value (Script S1). Linear mixed-effects modeling was performed to evaluate condition-dependent changes in emission ratio. Time-series emission ratio data from three biological replicates were exported to Excel and imported into MATLAB (R2025a). The time vector and three replicate traces were converted into long-format tables, in which each row corresponded to a single timepoint and its associated replicate identity. Three experimental conditions were defined according to the time windows of the recording: 0–20 min = Baseline, 20–40 min = Glucose treatment, and 40–60 min = Wash. The categorical condition assignments were replicated for each biological replicate. To account for replicate-to-replicate differences in baseline ratio levels, a linear mixed-effects model with a random intercept for each replicate was fitted:

$$\text{Emission Ratio}_{ij} \sim \text{Condition}_i + (1|\text{Replicate}_j).$$

The statistical framework for mixed-effects modeling follows established methods (Bates et al., 2015). Emission ratio measurements and interpretation were guided by methods for analyzing calcium activity in ventral pallidal GABAergic neurons as described previously (Scott et al., 2023). Model fitting was performed using fitlme (Statistics and Machine Learning Toolbox, MATLAB). Fixed-effect significance was assessed by ANOVA on the fitted model. Pairwise comparisons ('Baseline vs Glucose treatment', 'Glucose treatment vs Wash') were conducted as linear hypothesis tests using coefTest with the following contrast vectors:

$$\text{Baseline vs Glucose treatment} : [0\ \ 1\ \ 0].$$

$$\text{Glucose treatment vs Wash} : [0\ \ -1\ \ 1].$$

Time-course plots present the mean ± standard error (SE) across replicates, and the significance markers shown in the figures reflect the results of these LME contrasts (Script S2).

AUTHOR CONTRIBUTIONS

YI and WF conceived of the project. YI conducted all experiments. NZ and SP contributed to initial sensor construction. YI and WF prepared the figures. YI, NZ, and WF wrote the manuscript. NZ and SP validated maps and sequences.

ACKNOWLEDGEMENTS

This work is part of the collaboration research center CRC1535 funded by grants to WF from Deutsche Forschungsgemeinschaft (DFG, German Research Foundation)—Project 458090666/CRC1535 and Germany's Excellence Strategy—EXC-2048/1—project ID 390686111 (CEPLAS), and an Alexander von Humboldt Professorship. Open Access funding enabled and organized by Projekt DEAL.

DATA AVAILABILITY STATEMENT

The raw data have been deposited as an ARC under doi (available for publication). Plasmids are available from Addgene: pRSETb_MGlucoMeter2.6_7m (no. 247472), pRSETb_MGlucoMeter2.6_1m (no. 247471), pRSETb_MGlucoMeter2.6_700u (no. 247470), pRSETb_MGlucoMeter2.6_15u (no. 247469), pRSETb_MGlucoMeter2.6_353n (no. 247468).

SUPPORTING INFORMATION

Additional Supporting Information may be found in the online version of this article.

Table S1. Primers for DNA construction and mutagenesis.

Figure S1. Hydrogen bond interactions of two histidines with glucose in ttGBP (pdb 2B3B).

Figure S2. Predicted structure of MGlucoMeter2.6-1 m.

Figure S3. pH-dependent changes in the emission ratio of MGlucoMeter2.6 *in vitro*.

Figure S4. Time-dependent *in vivo* response of MGlucoMeter2.6-1 m in Arabidopsis roots, representing the second experimental replicate of the data presented in Figure 5.

Figure S5. Time-dependent *in vivo* response of MGlucoMeter2.6-1 m in Arabidopsis roots, representing the third experimental replicate of the data presented in Figure 5.

Figure S6. Fluorescence changes in individual channels for cpsfGFP and LSSmApple, corresponding to the results shown in Figure 6.

Figure S7. Detection of glucose accumulation in root tips of MGlucoMeter2.6-1 m expressing Arabidopsis seedlings in response to sucrose application to the cotyledons, representing the second experimental replicate of the data presented in Figure 6.

Figure S8. Detection of glucose accumulation in root tips of MGlucoMeter2.6-1 m expressing Arabidopsis seedlings in response to sucrose application to the cotyledons, representing the third experimental replicate of the data presented in Figure 6.

Figure S9. Quantification of emission ratio changes in different regions of MGlucoMeter2.6-1 m expressing roots.

Figure S10. Levels of cytosolic invertase CINV1 mRNA in cell types in the root tip derived from single cell sequencing data.

Text S1. Protein sequence of ttGBP polypeptide from *Thermus thermophilus* used for sensor construction.

Text S2. Protein sequence of MGlucoMeter.

Script S1. MATLAB script for curve fitting.

Script S2. MATLAB script for liner mixed-effects modeling.

Video S1. Time-dependent *in vivo* response of MGlucoMeter2.6-1 m in Arabidopsis roots.

Video S2. Detection of glucose accumulation in root tips of MGlucoMeter2.6-1 m expressing Arabidopsis seedlings in response to sucrose application to the cotyledons.

REFERENCES

Ast, C., **De Michele, R.**, **Kumke, M.U.** & **Frommer, W.B.** (2015) Single-fluorophore membrane transport activity sensors with dual-emission read-out. *eLife*, **4**, e07113.

Ast, C., **Foret, J.**, **Oltrogge, L.M.**, **De Michele, R.**, **Kleist, T.J.**, **Ho, C.-H.** ***et al.*** (2017) Ratiometric matryoshka biosensors from a nested cassette of green- and orange-emitting fluorescent proteins. *Nature Communications*, **8**, 431.

Baird, G.S., **Zacharias, D.A.** & **Tsien, R.Y.** (1999) Circular permutation and receptor insertion within green fluorescent proteins. *Proceedings of the National Academy of Sciences of the United States of America*, **96**, 11241–11246.

Barratt, D.H., **Derbyshire, P.**, **Findlay, K.**, **Pike, M.**, **Wellner, N.**, **Lunn, J.** ***et al.*** (2009) Normal growth of Arabidopsis requires cytosolic invertase but not sucrose synthase. *Proceedings of the National Academy of Sciences of the United States of America*, **106**, 13124–13129.

Bates, D., **Mächler, M.**, **Bolker, B.** & **Walker, S.** (2015) Fitting linear mixed-effects models using lme4. *Journal of Statistical Software*, **67**, 1–48. Available from: https://doi.org/10.18637/jss.v067.i01

Bermejo, C., **Ewald, J.C.**, **Lanquar, V.**, **Jones, A.M.** & **Frommer, W.B.** (2011) In vivo biochemistry: quantifying ion and metabolite levels in individual cells or cultures of yeast. *Biochemical Journal*, **438**, 1–10.

Bermejo, C., **Haerizadeh, F.**, **Sadoine, M.S.**, **Chermak, D.** & **Frommer, W.B.** (2013) Differential regulation of glucose transport activity in yeast by specific cAMP signatures. *Biochemical Journal*, **452**, 489–497.

Bermejo, C., **Haerizadeh, F.**, **Takanaga, H.**, **Chermak, D.** & **Frommer, W.B.** (2010) Dynamic analysis of cytosolic glucose and ATP levels in yeast using optical sensors. *Biochemical Journal*, **432**, 399–406.

Bermejo, C., **Haerizadeh, F.**, **Takanaga, H.**, **Chermak, D.** & **Frommer, W.B.** (2011) Optical sensors for measuring dynamic changes of cytosolic metabolite levels in yeast. *Nature Protocols*, **6**, 1806–1817.

Chaudhuri, B., **Hörmann, F.** & **Frommer, W.B.** (2011) Dynamic imaging of glucose flux impedance using FRET sensors in wild-type Arabidopsis plants. *Journal of Experimental Botany*, **62**, 2411–2417.

Chaudhuri, B., **Hörmann, F.**, **Lalonde, S.**, **Brady, S.M.**, **Orlando, D.A.**, **Benfey, P.** ***et al.*** (2008) Protonophore- and pH-insensitive glucose and sucrose accumulation detected by FRET nanosensors in Arabidopsis root tips. *The Plant Journal*, **56**, 948–962.

Cleveland, W.S. & **Devlin, S.J.** (1988) Locally weighted regression: an approach to regression analysis by local fitting. *Journal of the American Statistical Association*, **83**, 596–610.

Cuneo, M.J., **Beese, L.S.** & **Hellinga, H.W.** (2009) Structural analysis of semi-specific oligosaccharide recognition by a cellulose-binding protein of *Thermotoga maritima* reveals adaptations for functional diversification of the oligopeptide periplasmic binding protein fold. *Journal of Biological Chemistry*, **284**, 33217–33223.

De Michele, R., **Ast, C.**, **Loque, D.**, **Ho, C.-H.**, **Andrade, S.L.A.**, **Lanquar, V.** ***et al.*** (2013) Fluorescent sensors reporting the activity of ammonium transceptors in live cells. *eLife*, **2**, e00800.

Deuschle, K., **Chaudhuri, B.**, **Okumoto, S.**, **Lager, I.**, **Lalonde, S.** & **Frommer, W.B.** (2006) Rapid metabolism of glucose detected with FRET glucose nanosensors in epidermal cells and intact roots of Arabidopsis RNA-silencing mutants. *Plant Cell*, **18**, 2314–2325.

Deuschle, K., **Okumoto, S.**, **Fehr, M.**, **Looger, L.L.**, **Kozhukh, L.** & **Frommer, W.B.** (2005) Construction and optimization of a family of genetically encoded metabolite sensors by semirational protein engineering. *Protein Science*, **14**, 2304–2314.

Ejike, J.O., **Sadoine, M.**, **Shen, Y.**, **Ishikawa, Y.**, **Sunal, E.**, **Hänsch, S.** ***et al.*** (2024) A monochromatically excitable green–red dual-fluorophore fusion incorporating a new large stokes shift fluorescent protein. *Biochemistry*, **63**, 171–180. Available from: https://doi.org/10.1021/acs.biochem.3c00451

Fehr, M., **Frommer, W.B.** & **Lalonde, S.** (2002) Visualization of maltose uptake in living yeast cells by fluorescent nanosensors. *Proceedings of the National Academy of Sciences of the United States of America*, **99**, 9846–9851.

Fehr, M., **Lalonde, S.**, **Lager, I.**, **Wolff, M.W.** & **Frommer, W.B.** (2003) In vivo imaging of the dynamics of glucose uptake in the cytosol of COS-7 cells by fluorescent nanosensors. *Journal of Biological Chemistry*, **278**, 19127–19133.

Fehr, M., **Takanaga, H.**, **Ehrhardt, D.W.** & **Frommer, W.B.** (2005) Evidence for high-capacity bidirectional glucose transport across the endoplasmic reticulum membrane by genetically encoded fluorescence resonance energy transfer nanosensors. *Molecular and Cellular Biology*, **25**, 11102–11112.

Kaper, T., **Lager, I.**, **Looger, L.L.**, **Chermak, D.** & **Frommer, W.B.** (2008) Fluorescence resonance energy transfer sensors for quantitative monitoring of pentose and disaccharide accumulation in bacteria. *Biotechnology for Biofuels*, **1**, 11.

Keller, J.P., **Marvin, J.S.**, **Lacin, H.**, **Lemon, W.C.**, **Shea, J.**, **Kim, S.** ***et al.*** (2021) *In vivo* glucose imaging in multiple model organisms with an engineered single-wavelength sensor. *Cell Reports*, **35**, 109284.

Lager, I., **Looger, L.L.**, **Hilpert, M.**, **Lalonde, S.** & **Frommer, W.B.** (2006) Conversion of a putative *agrobacterium* sugar-binding protein into a FRET sensor with high selectivity for sucrose. *Journal of Biological Chemistry*, **281**, 30875–30883.

Pedelacq, J.D., **Cabantous, S.**, **Tran, T.**, **Terwilliger, T.C.** & **Waldo, G.S.** (2006) Engineering and characterization of a superfolder green fluorescent protein. *Nature Biotechnology*, **24**, 79–88.

Peragine, A., **Yoshikawa, M.**, **Wu, G.**, **Albrecht, H.L.** & **Poethig, R.S.** (2004) SGS3 and SGS2/SDE1/RDR6 are required for juvenile development and the production of trans-acting siRNAs in Arabidopsis. *Genes & Development*, **18**, 2368–2379.

Rowe, J.H., **Rizza, A.** & **Jones, A.M.** (2022) Quantifying Phytohormones in vivo with FRET biosensors and the FRETENATOR analysis toolset. In: Duque, P. & Szakonyi, D. (Eds.) *Environmental Responses in Plants: Methods and Protocols*. New York, NY: Springer US, pp. 239–253. Available from: https://doi.org/10.1007/978-1-0716-2297-1_17

Schindelin, J., **Arganda-Carreras, I.**, **Frise, E.**, **Kaynig, V.**, **Longair, M.**, **Pietzsch, T.** ***et al.*** (2012) Fiji: an open-source platform for biological-image analysis. *Nature Methods*, **9**, 676–682.

Scott, A., **Palmer, D.**, **Newell, B.**, **Lin, I.**, **Cayton, C.A.**, **Paulson, A.** ***et al.*** (2023) Ventral pallidal GABAergic neuron calcium activity encodes cue-driven reward seeking. *Journal of Neuroscience*, **43**, 5191–5203. Available from: https://doi.org/10.1523/JNEUROSCI.0013-23.2023

Stadler, R., **Wright, K.M.**, **Lauterbach, C.**, **Amon, G.**, **Gahrtz, M.**, **Feuerstein, A.** ***et al.*** (2005) Expression of GFP-fusions in Arabidopsis companion cells reveals non-specific protein trafficking into sieve elements and identifies a novel post-phloem domain in roots. *The Plant Journal*, **41**, 319–331.

Takanaga, H., **Chaudhuri, B.** & **Frommer, W.B.** (2008) GLUT1 and GLUT9 as major contributors to glucose influx in HepG2 cells identified by a high sensitivity intramolecular FRET glucose sensor. *Biochimica et Biophysica Acta*, **1778**, 1091–1099.

Wright, K.M. & **Oparka, K.J.** (1997) Metabolic inhibitors induce symplastic movement of solutes from the transport phloem of Arabidopsis roots. *Journal of Experimental Botany*, **48**, 1807–1814.